

## RESEARCH ARTICLE

10.1029/2018JC013868

This article is a companion to Banyte et al. (2018), <https://doi.org/10.1029/2018JC013869>

## Key Points:

- The single abyssal water source for the Panama Basin is the flow through the Ecuador Trench
- Critical flow theory suggests an abyssal water inflow of  $0.29 \pm 0.07$  Sv
- The effect of geothermal heating can reach as high as 2,200-m depth or 500 m above the abyssal water layer

## Correspondence to:

D. Banyte,  
[donata.banyte@newcastle.ac.uk](mailto:donata.banyte@newcastle.ac.uk)

## Citation:

Banyte, D., Morales Maqueda, M., Hobbs, R., Smeed, D. A., Megann, A., & Recalde, S. (2018). Geothermal heating in the Panama Basin: 1. Hydrography of the basin, *Journal of Geophysical Research: Oceans*, 123, 7382–7392. <https://doi.org/10.1029/2018JC013868>

Received 1 FEB 2018

Accepted 21 MAY 2018

Accepted article online 24 AUG 2018

Published online 21 OCT 2018

## Geothermal Heating in the Panama Basin: 1. Hydrography of the Basin

D. Banyte<sup>1</sup> , M. Morales Maqueda<sup>1</sup>, R. Hobbs<sup>2</sup> , D. A. Smeed<sup>3</sup> , A. Megann<sup>3</sup> , and S. Recalde<sup>4</sup>

<sup>1</sup>School of Marine Science and Technology, Newcastle University, Newcastle, UK, <sup>2</sup>Department of Earth Sciences, Durham University, Durham, UK, <sup>3</sup>National Oceanography Centre, Southampton, UK, <sup>4</sup>Instituto Oceanográfico de la Armada, Guayaquil, Ecuador

**Abstract** The Panama Basin serves as a laboratory to investigate abyssal water upwelling. The basin has only a single abyssal water inflow pathway through the narrow Ecuador Trench. The estimated critical inflow through the Trench reaches  $0.34 \pm 0.07$  m/s, resulting in an abyssal water volume inflow of  $0.29 \pm 0.07$  Sv. The same trench carries the return flow of basin waters that starts just 200 m above the bottom and is approximately 400-m deeper than the depth of the next possible deep water exchange pathway at the Carnegie Ridge Saddle. The curvature of temperature-salinity diagrams is used to differentiate the effect of geothermal heating on the deep Panama Basin waters that was found to reach as high as 2,200-m depth, which is about 500 m above the upper boundary of the abyssal water layer.

### 1. Introduction

The contribution of geothermal heating to global abyssal water transformation is currently highly debated, and estimates range from insignificant to over 30% (Adcroft et al., 2001; de Lavergne et al., 2016; Emile-Geay & Madec, 2009; Hofmann & Morales Maqueda, 2009). In addition, the thermodynamic effect of the geothermal heating on bottom waters is predicted by models to be significant, exceeding  $0.1$  °C (Downes et al., 2016). In observational studies, the geothermal heating signature on abyssal water hydrography is clearly demonstrated for waters over hydrothermal plumes, the *hot springs* with source temperatures of several hundred degrees, discharged from the oceanic crust (e.g., Baker & Massoth, 1987; Murton et al., 2006). Over plumes, a temperature-salinity (TS) anomaly can extend several hundreds of meters above the bottom. However, away from active hydrothermal vents, it is often difficult to attribute enhancement of bottom temperatures to weak geothermal heating. As a result, the geothermal heating effect on the large-scale hydrography of ocean basins is poorly documented in observations.

The Panama Basin is a perfect laboratory to investigate the geothermal heating effect on abyssal water upwelling. It is relatively small, has a single narrow abyssal water inflow passage, the Ecuador Trench about 2,900 m deep, but is completely closed below 2,300 m from the rest of the tropical Pacific Ocean and is the site of stronger than average geothermal heating.

In the early 1970s, the Panama Basin was singled out to investigate geothermal heating. Having 24 full depth profiles, Laird (1971) mapped the basins hydrography, noting the presence of horizontal temperature gradients in the bottom water, but failed to observe the bottom salinity gradients. As salinity is decreasing with height for abyssal waters in the basin, he argued that increase in bottom temperature with no observed decrease in bottom salinity is a consequence of strong geothermal heating. In addition, Detrick et al. (1974) inferred that active spreading ridges in the basin might induce a substantial hydrothermal circulation from observations of large temperature anomalies just meters above the ridge, even though they found no anomalies in the range of 50 m to 200 m above the bottom.

Believing that the deep Panama Basin waters can only escape from the basin through the shallow and broad Carnegie Ridge Saddle located at  $86^{\circ}$ W and 2,300-m depth, Detrick et al. (1974) compared the heat advected out of the basin with the total geothermal heat gain estimate. They raised the hypothesis of geothermal heating being the driver for abyssal overturning. However, current meter measurements showed no significant outflow at the Carnegie Ridge Saddle (Lonsdale, 1977). On the contrary, sediment ripple marks downstream of this passage indicated that deep waters could inflow into the basin, at least occasionally. However, the inflow

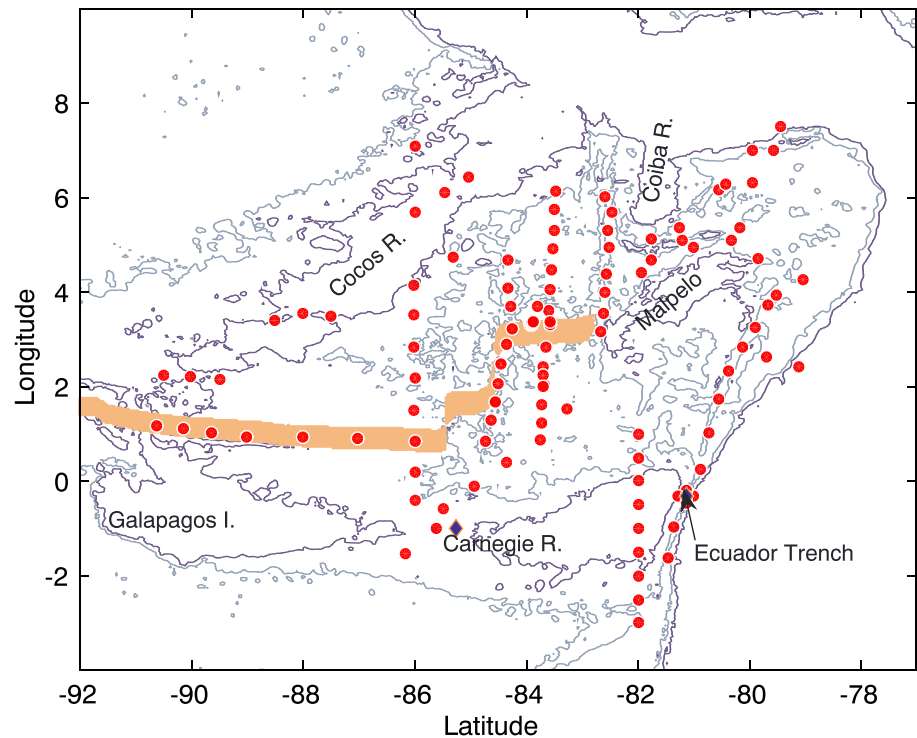


**Figure 1.** The bathymetry of the Panama Basin. Red dots show locations of conductivity-temperature-depth casts collected between December 2014 and March 2015, blue diamonds show locations of moored acoustic Doppler current profilers. Bathymetry contours mark the depths of 2,000 m and 3,000 m. The thick, brown line marks the location of geothermal heating larger than  $500 \text{ mW/m}^2$ .

must also be weak judging from the current meter evidence (Lonsdale, 1977) and higher silica values inside the basin than upstream of the Carnegie Ridge Saddle (Tsuchiya & Talley, 1998).

In this study, we investigate the hydrographic evidences for the geothermal heating of deep waters in the Panama Basin. For this purpose, we analyze the hydrographic data near two deep water exchange passages: the Ecuador Trench and the Carnegie Ridge Saddle. The inflow estimates are computed using the methodology of (Lonsdale, 1977), who lacked salinity measurements, while evidence for deep water inflow through the Carnegie Ridge Saddle is investigated with the oxygen data (section 3). Positive anomalies of temperature and salinity, the signatures of geothermal heating, are observed below 2,200 m in the Panama Basin (section 4).

## 2. Data

All observational data used in this study were collected from December 2014 to March 2015 in the cruises JC112 on RRS *James Cook* and SO238 on FS *Sonne*, as part of the multidisciplinary research project OSCAR (Oceanographic and Seismic Characterization of heat dissipation and alteration by hydrothermal fluids at an Axial Ridge), which aims to investigate the coupling of hydrothermal flow between the ocean and the lithosphere; its impact on the evolution of the oceanic crust and on basin-scale circulation.

During JC112, the western side of the basin was sampled. This is a region of intensive geothermal heat released by several oceanic spreading ridges (Figure 1). Overall, there were 87 conductivity-temperature-depth (CTD) casts, all taken down to approximately 5 m above the bottom. SO238 focused on the eastern part of the basin, which is the region of densest bottom waters with the single abyssal water inflow pathway through the Ecuador Trench. In total, there were 45 full depth CTD casts in this second cruise. The vertical distributions of temperature, salinity, and dissolved oxygen down to the bottom were measured with a SBE911plus CTD system (Sea-Bird Electronics, Inc.). The accuracy of the sensors was  $0.001 \text{ }^\circ\text{C}$ ,  $0.0003 \text{ S/m}$ ,  $1 \text{ dB}$ , and  $0.1 \text{ ml/L}$  ( $4.47 \text{ } \mu\text{mol/kg}$ ) for temperature, conductivity, pressure, and oxygen, respectively. The temperature and salinity in this study are reported as Conservative Temperature and Absolute Salinity as computed using the Gibbs SeaWater (GSW) Oceanographic Toolbox of TEOS-10 (McDougall & Barker, 2011).

A 75-kHz upward looking acoustic Doppler current profiler (ADCP) was moored on the crest of the sill of the Ecuador Trench for 24 hr at a depth of 2,921 m. Another 75-kHz ADCP was moored on the central saddle of Carnegie Ridge for about 2 months at a depth of 2,300 m (Figure 1).

### 3. Geography of the Basin

#### 3.1. Topography

The Panama Basin is separated from the rest of the tropical Pacific Ocean by the Cocos Ridge, the Galapagos Platform, and the Carnegie Ridge (Figure 1). The ridges form a complete barrier below about 2,300 m, except for the narrow trench near the coast of Ecuador with a sill at 2,930 m. The Carnegie Ridge Saddle, approximately 2,300-m deep and located at 86°W, allows deep water exchange with the surrounding tropical Pacific Ocean. Inside the Panama Basin, two small ridges, Coiba and Malpelo, divide the basin into eastern and western parts. The Costa Rica, Ecuador, and Galapagos rifts, located on the western part of the Panama Basin, release geothermal heating as high as 1 W/m<sup>2</sup>, with the basin average being 220 mW/m<sup>2</sup>. The geothermal heatflux in the basin was estimated from the age map of the ocean floor (Müller et al., 1997), as a proxy for the heat flow using the Stein and Stein (1992) formula, which links the age of the bedrock to the heat flow through the crust:  $q(t) = 510t^{-0.5}$ , where  $t$  is crust age in Myr (million years) and  $q$  is the heat flow in mW/m<sup>2</sup> (milliwatt per square meter).

#### 3.2. Deep Water Exchange Through the Ecuador Trench

The Ecuador Trench was described in detail by Lonsdale (1977) as being terraced with steep fault scarps that channel deep waters in a zigzag fashion. He estimated the abyssal water inflow rate through the passage by applying hydraulic critical control theory, but used only temperature data. Here we employ our high-resolution data to recalculate the inflow parameters for the Ecuador Trench.

Hydraulic theory of rotating and nonrotating flow past topographic constrictions such as dams, weirs, and channels has been described by Whitehead et al. (1974). For the Ecuador Trench, the maximal transport derivation for nonrotational flow over a weir can be applied, because the Trench is situated within a degree of the equator and the internal Rossby radius is much larger than the width of the Trench (about 6 km at 2,700 m depth). The maximum velocity ( $v_0$ ) of abyssal water inflow then is expressed as

$$v_0 = \sqrt{g'h_0},$$

where

$$g' = g(\gamma_b - \gamma_u)/(\gamma_b)$$

is *reduced gravity*,  $\gamma_b$  is neutral density (Jackett & McDougall, 1997) at the bottom of the Trench (or bottom of the inflow), while  $\gamma_u$  marks the top of the inflow at the Trench. Thus, an estimate of maximum velocity of bottom waters entering the Panama Basin depends on the estimate of density and pressure of the top layer of the inflow. The OSCAR data set has one profile placed directly at the crest, two casts upstream and two casts downstream from the crest (Figure 2).

At the crest of the Ecuador Trench, the highest density of the inflow was found to be  $\gamma_b = 28.016$  kg/m<sup>3</sup> at the depth of 3,050 m. The high-resolution ship-based multibeam echo sounder reveals that the shallowest part of the Ecuador Trench is located at 0.36°S at a depth of 2,930 m (Figure 3). The CTD profile at this location shows that the water between 2,200 and 2,680 m is more weakly stratified than the water below. This is the first indication that there is an outflow of homogenized Panama Basin water through the trench. That the water at 2,200 m is denser inside the basin than out also supports this assertion. Consequently, we set the upper boundary of the inflow at 2,680 m with corresponding neutral density  $\gamma_u = 27.967 \pm 0.002$  kg/m<sup>3</sup> (Figure 2). Upstream of the sill, the neutral density surface  $\gamma_u$  is positioned at the higher depth of 2,510 m.

Thus, the thickness of abyssal inflow at the crest is estimated to be  $h_0 = 2,930 - 2,680 = 250$  (m), while upstream it is:  $h_u = 2,930 - 2,510 = 420$  (m). For hydraulically controlled flows the height of the top of the inflow at the crest ( $h_0$ ) is lower than upstream ( $h_u$ ) by approximately one-third (Whitehead et al., 1974): the criterion that is observed in our data as well. Taking the 'reduced gravity' as:  $g' = 9.81 \times (1,028.016 - 1,027.967)/1,028.016 = 0.47 \times 10^{-3}$  (m/s<sup>2</sup>), the maximum inflow velocity is estimated to be:

$$v_0 = \sqrt{0.47 \times 10^{-3} \times 250} = 0.34 \text{ (m/s)}.$$

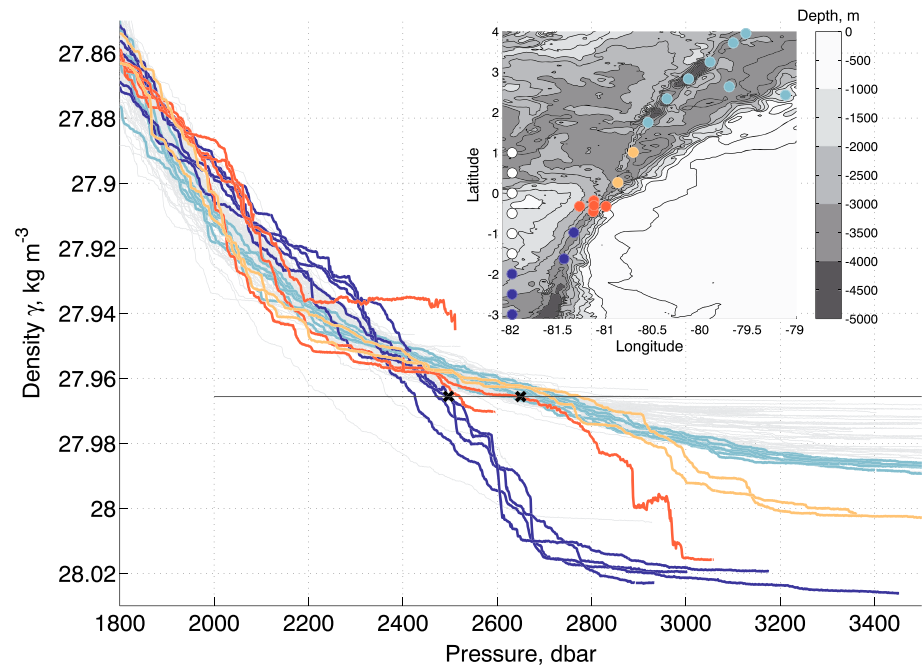


**Figure 2.** Stratification profiles at the Ecuador Trench, where a cluster of five stations are situated directly at the crest of the Trench. Crosses mark the density and depth of the top of the inflow layer directly at the crest (red curve) and upstream (blue curves). Profiles from the rest of the basin are marked in gray.

In comparison, Lonsdale (1977) found the upper boundary of the inflow to be 60 m shallower, at 2,620 m, with the upstream depth of the same isotherm extending to 2,500 m (similar to our observation). However, his estimates of the average depth of the Ecuador Trench is also shallower by about 80 m and taken as 2,850 m. Using the modern topography data, the critical flow height is recomputed to be 310 m at the crest and 430 m upstream. Furthermore, due to a lack in salinity measurements, Lonsdale (1977) estimated reduced gravity to be almost half that observed in our study. With our estimate of  $g'$  and a critical height estimate corrected for the depth of the Trench, the historical data of Lonsdale (1977) results in a critical flow velocity of 0.39 m/s, which is larger than his original estimate of 0.25 m/s, but also closer to our estimate of 0.34 m/s. Furthermore, his current meter measurements yielded the average inflow velocity of 0.33 m/s, which is in a good agreement with our critical flow estimate.

To get a feeling of the uncertainty of  $v_0$  estimated using the hydraulic control method, we set the uncertainty of the total height of the inflow at 100 m. This leads to an uncertainty of 20%, or 0.07 m/s, for  $v_0$ .

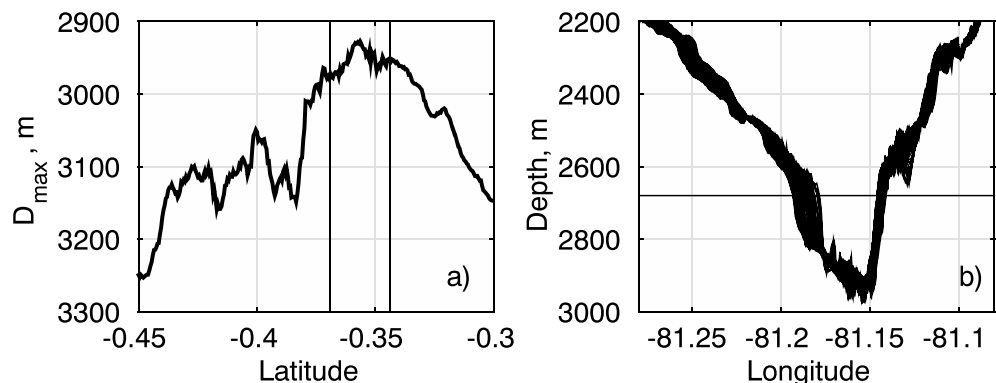


**Figure 3.** (a) The maximum depth along multiple zonal transects derived from echo sounding data, where gray vertical lines mark a 3-km distance centered at the crest of the Ecuador Trench. (b) Ensemble of 50 zonal multibeam profiles within the region bound by the vertical lines shown in (a). Horizontal line marks the depth of the estimated upper boundary of the abyssal inflow.

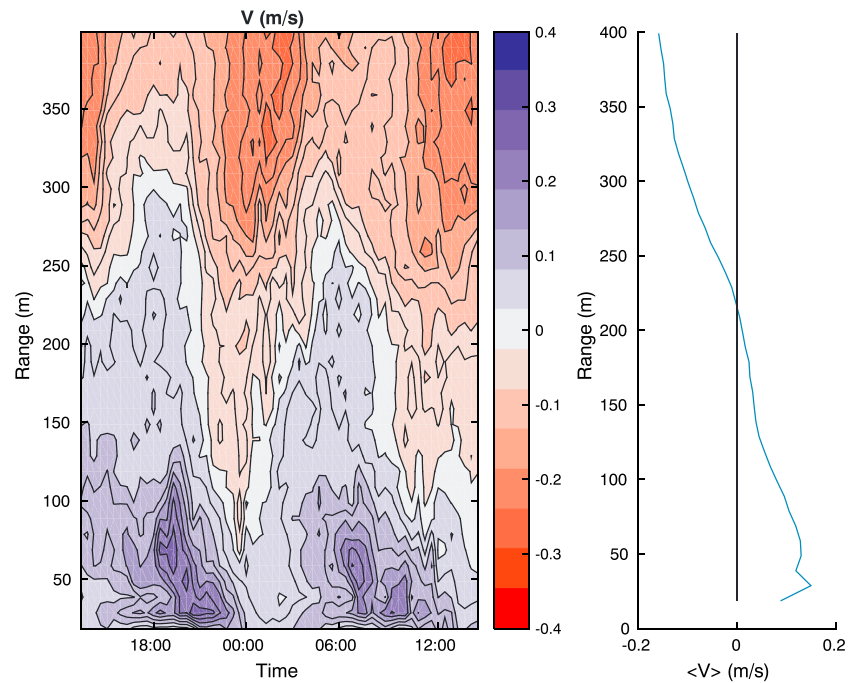


**Figure 4.** 24 hour velocity measurements by bottom moored ADCP at the crest of the Ecuador Trench: (left) instantaneous velocities, (right) isobarically averaged velocities.

The cross-section area of the trench at the crest of the sill below 2,680 m is  $0.84 \pm 0.05 \text{ km}^2$  (Figure 3). The cross-section area uncertainty was computed from 50 multibeam profiles, as shown in Figure 3 (b). The resulting total inflow of abyssal waters through the Ecuador passage is  $0.29 \pm 0.07 \text{ Sv}$ .

Additional evidence for the deep water inflow and outflow through the Ecuador Trench comes from velocity measurements of bottom ADCP moored directly at the crest of the trench. The 75-kHz upward looking ADCP measured currents for 24 hr (Figure 4). The strongest measured northward velocities in the lower 100 m were above 0.3 m/s. Similar maximum speeds were measured 300 m above the bottom for the southward currents (outflow). The average velocities during a short measurement period were less than 0.2 m/s for both northward and southward currents. Even though a much longer ADCP deployment period is needed for a more robust estimate of the flows, the observations reasonably well agree with the velocity estimate derived using hydraulic control theory.

Finally, support for the outflow through the Ecuador Trench comes also from the TS identity of those waters. Directly at the crest of the Trench, the TS profiles shift toward higher temperatures in the depth range between 2,700 m and 2,200 m (marked by black crosses in Figure 5). In other words, in this density range, the water masses observed directly at the crest resemble waters downstream from the crest. We note that Lonsdale (1977) also found substantial velocities for this water layer, but did not explicitly state its direction, nor importance as a route for deep Panama Basin waters to leave the basin.

### 3.2.1. Inflow Through the Carnegie Ridge Saddle

Above 2,300 m, the topography allows for the first deep water exchange other than through the Ecuador Trench. The flow through the Carnegie Ridge Saddle from current meters was found to be very weak (Lonsdale, 1977), and only geological evidence suggests the direction of the flow to be into the basin (Lonsdale & Malfait, 1974). We looked at oxygen profiles to search for evidence of the inflow (Figure 6).

The Panama basin, as part of the eastern tropical Pacific Ocean, has a hypoxic zone in the thermocline at about 400-m depth, where oxygen concentrations drop below  $2 \mu\text{mol/kg}$ . Farther down, oxygen concentrations are gradually increasing. Unlike temperature or salinity, oxygen is a nonconservative tracer as it is consumed by aerobic respiration; the higher the age of the water mass the less oxygen it contains. Thus, a new source of deep waters entering the basin, such as an inflow over the Carnegie Ridge, is expected to have an elevated oxygen concentration when compared with the waters inside the basin.

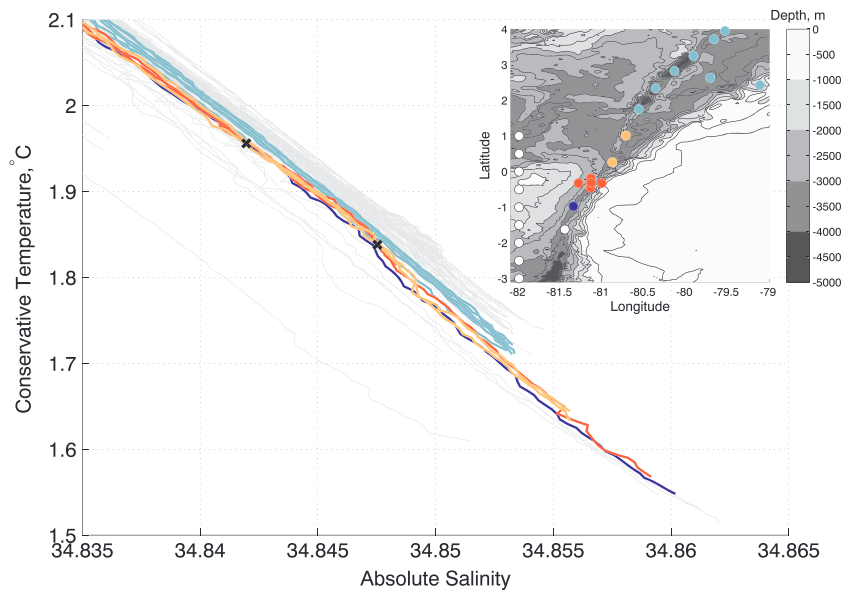


**Figure 5.** Temperature-salinity diagram at the inflow region. Shown in gray are all other profiles collected during OSCAR cruises.

In the vicinity of the Carnegie Ridge, the oxygen concentrations are elevated above the  $\gamma_{27.97}$  isopycnal (Figure 6). An especially strong oxygen signal is observed in the density range  $\gamma = [27.96 \text{--} 27.95] \text{ kg/m}^3$ , corresponding to the depth range of 2,300–2,600 m. However, just 100 km away from the ridge, the oxygen concentration peak disappears for that water mass as seen in the profiles along the 1°N transect. Lateral advection and turbulent mixing effectively destroy a sharp oxygen gradient. A tongue of high oxygen concentrations is an evidence for the water inflow through the shallower deep water passage. The higher oxygen signal is also accompanied by a lower salinity signal. Hence, the southern boundary is the source for low-salinity waters.

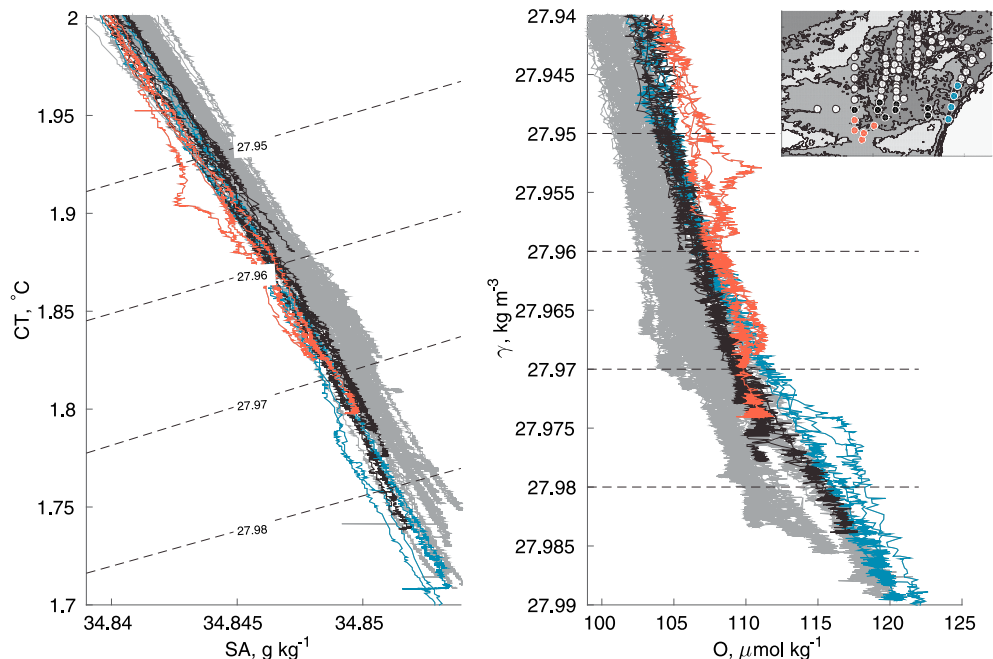


**Figure 6.** Temperature-salinity diagram (left) and oxygen-density profiles (right) inside the basin (gray), in the vicinity of the Ecuador Trench (blue), along a section centered at 1°N (black), and in the vicinity of the Carnegie Ridge Saddle (red).

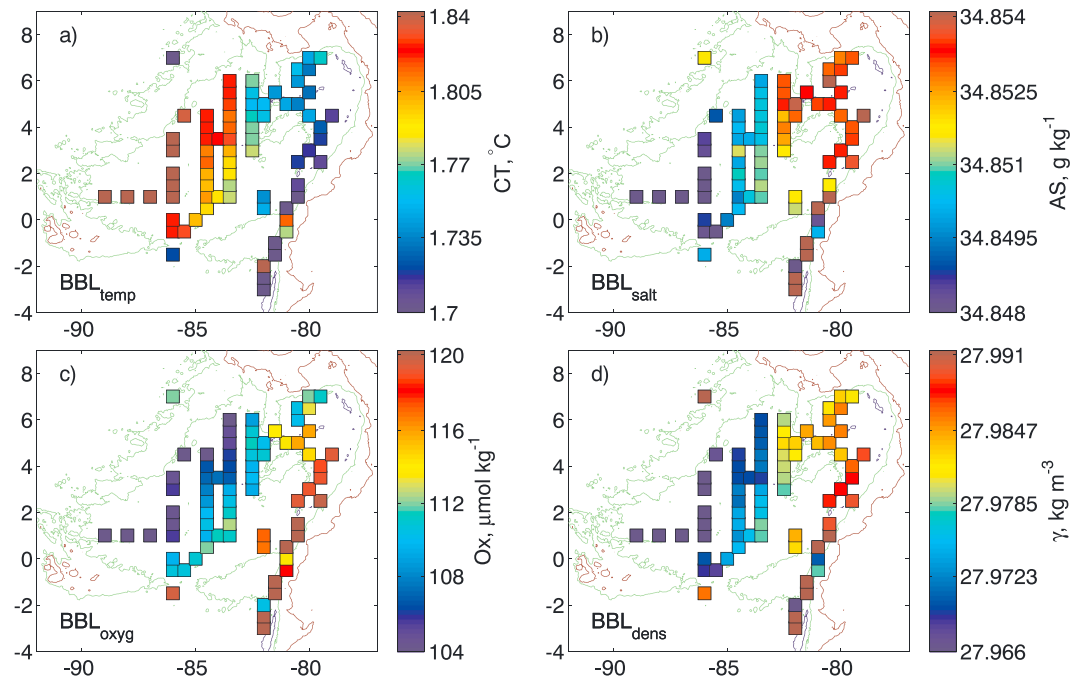


**Figure 7.** Hydrographic properties of bottom water: (a) conservative temperature, (b) absolute salinity, (c) oxygen, (d) neutral density. The data of bottom moist 50 m were averaged and then gridded to  $0.5^\circ \times 0.5^\circ$  spatial grid. The green contours show the 2,200-m depth isobath.

However, the moored ADCP instrument installed directly at the crest for almost 2 months failed to provide evidence for a persistent inflow, similarly to measurements of Lonsdale (1977). Alternating northward/eastward velocities of up to  $0.1 \text{ m/s}^1$  and on average less than  $0.02 \text{ m/s}^1$  were recorded (not shown). While we can not deduce the volume flux through the Carnegie Ridge Saddle, but from the weak persistent velocity measurements we judge the volume flux to be weak.

#### 4. Abyssal Hydrography

##### 4.1. The Positive Anomaly of Temperature and Salinity

Abyssal waters in the Panama Basin originate as overflow through the narrow Ecuador Trench at the southeast corner of the basin. As was estimated above, the abyssal water layer is bound in the vertical by the bottom and the  $\gamma = 27.967 \text{ kg/m}^3$  isopycnal, which is located at a depth of 2,680 m in the vicinity of the Ecuador Trench, but at 3,000 m in the western side of the basin. Over a distance of 200 km downstream of the trench, abyssal waters experience extreme water mass transformation as the densest waters become rapidly lighter by about  $0.028 \text{ kg/m}^3$  (Figure 2). This corresponds to a warming of  $0.15^\circ\text{C}$ , which is the most intense abyssal water warming than anywhere else observed in the interior of the basin. Hydraulic flow theory of narrow passages predicts hydraulic jumps and resulting strong mixing downstream of such channels (e.g., Alford et al., 2013; St Laurent & Thurnherr, 2007). Hence, the observed intense warming of densest waters is a signature of critical flow, even though hydraulic jumps were not directly observed in our data.

Once they have passed through the intense mixing region of the Ecuador Trench, abyssal waters spread from the eastern to the western side of the basin, gradually becoming lighter and older (Figure 7). In general, lighter waters have higher temperatures and lower salinities (Figure 5), a common characteristics of Pacific Ocean deep waters. In addition, older waters are depleted of oxygen, even though the oxygen consumption at depth is much weaker than at the surface. Hence, from the east to the west, the bottom waters become lighter, warmer, fresher, and less oxygenated. While a similar pattern was reported by Laird (1971), poor quality salinity data did not allow him to observe the reduction in bottom salinities in the western side of the basin.

However, it is not the salinity decrease for bottom waters, but salinity increase along the density surfaces, that is the main indication of geothermal heating. Geothermal heating, unlike turbulent mixing, is an external forcing; it introduces salinity as well as temperature anomalies in abyssal waters. The temperature and salinity anomalies, introduced by the raising water parcels heated at the bottom, depend on the water column

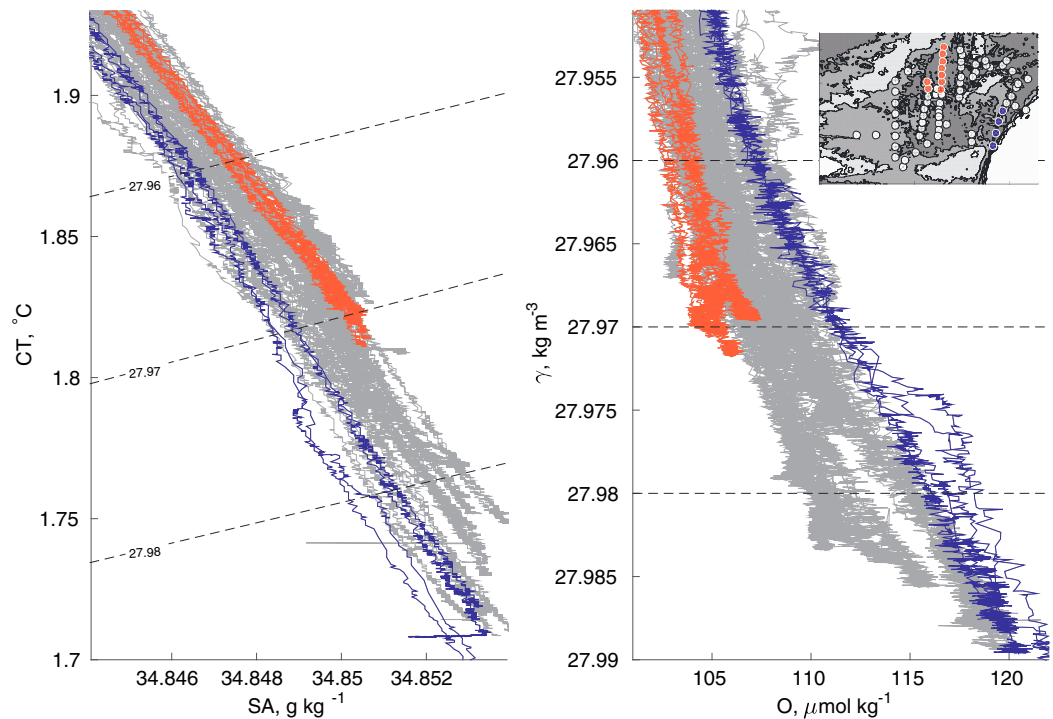


**Figure 8.** Temperature-salinity diagram (a) and oxygen versus neutral density profiles (b) at the source of abyssal waters (blue) and over the region where abyssal waters are the oldest (red). Shown in gray are all other profiles located inside the basin. The three neutral densities are marked, where  $27.967 \text{ kg/m}^3$  is the upper boundary of abyssal water layer.

stability ratio (e.g., Bindoff & Mcdougall, 1994; Speer & Rona, 1989). In the Pacific, with a stable background salinity gradient, the *purely* heated water parcel rises and mixes with surrounding waters that are colder, but also fresher. When a heated water parcel reaches its height of neutral buoyancy, it is still warmer, but also saltier than the surroundings. Hence, basal heating of the deep Panama Basin waters introduces positive both temperature and salinity anomalies.

When following water properties along density surfaces, the positive temperature anomaly of deep basin waters is accompanied by a positive salinity anomaly on the western side of the basin (Figure 8). A positive temperature anomaly of  $0.0074 \text{ }^\circ\text{C}$ , a positive salinity anomaly of  $0.0015 \text{ g/kg}$ , and a negative oxygen anomaly of  $6.57 \text{ } \mu\text{mol/kg}$  are observed on the western side of the basin along the isopycnal  $\gamma = 27.967 \text{ kg/m}^3$ , which is the upper boundary of the abyssal water layer. The above lying deep waters are warmer and fresher; hence, the positive salinity anomaly cannot be explained by diapycnal turbulent mixing. In the absence of lateral inflows, the positive salinity anomaly can, therefore, only be explained by the geothermal heating.

#### 4.2. Vertical Extent of the Geothermal Heating Effect

The geothermal heating from the bottom is transported upward either through small-scale turbulent mixing or water transport across density surfaces. The most distinct signal of upward propagating TS anomalies is found directly over hot spots of geothermal heating, such as the Costa Rica Rift. Directly over the Costa Rica Rift, the distinct TS anomalies extend about 500 m upward starting from the upper boundary of the abyssal water layer, up to the isopycnal  $\gamma = 27.960 \text{ kg/m}^3$  (Figure 9), corresponding to the depth of 2,500 m. Importantly, though, in the bottom mixed layer the local water properties over the Costa Rica Rift fully comply with the TS properties of the surrounding abyssal waters, indicating that spatial mixing at the bottom mixed layer is very intense, as expected. Above the bottom mixed layer, the water stratification is still very weak allowing for the heating signal to reach extensive height. However, the distinct concave signature in the TS diagram caused by extensive geothermal heating is not seen in the profiles just 50 km away. Both isopycnal and diapycnal mixing effectively tend to smooth out local TS anomalies, by spreading those anomalies both laterally and vertically.

However, the large-scale accumulative effect of geothermal heating can be observed by comparing deep Panama Basin waters with surrounding tropical Pacific waters. Tsuchiya and Talley (1998) find a divergence of

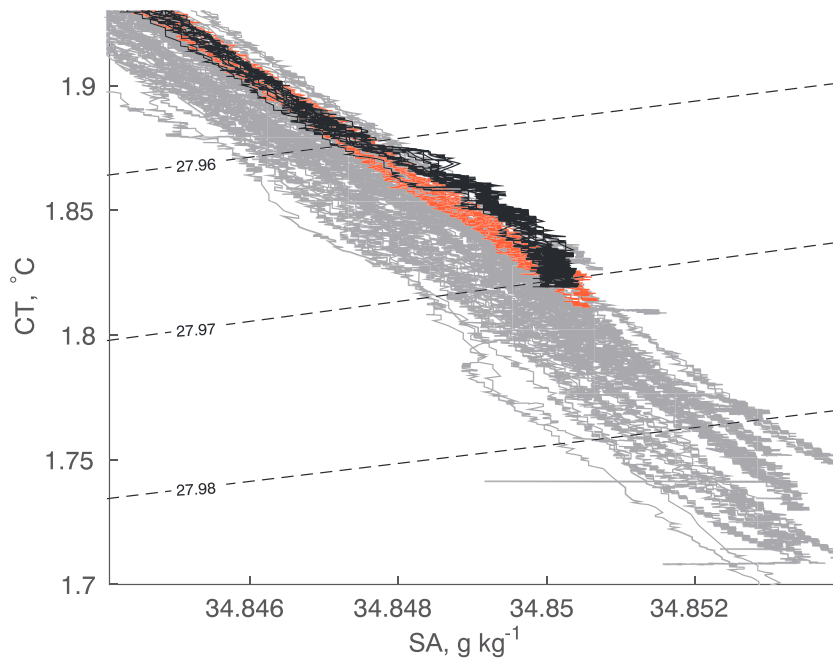


**Figure 9.** Temperature-salinity diagram for all inner basin profiles (gray), directly at the Costa Rica Rift with 50-km radius (black), and in the vicinity of the Rift with 100-km radius (red).

hydrographic properties inside the Panama Basin, when crossing from the Guatemala Basin to the Peru Basin. Below about 2,200 m, much lighter density, warmer and fresher waters are found within the Panama Basin than outside the basin. Here we look at the hydrographic properties of the outflow waters at the Ecuador Trench. The outflow was identified by the change in stratification in the depth range 2,200–2,700 m. Above this depth range, up to isopycnal  $\gamma = 27.825 \text{ kg/m}^3$  (1,700 m), the TS profiles are almost linear, while farther up—they gain a prominent convex form. At the range of estimated deep water outflow, the TS profiles are concave: bent to higher temperatures and salinities (Figure 10). Hence, assuming no significant inflow into

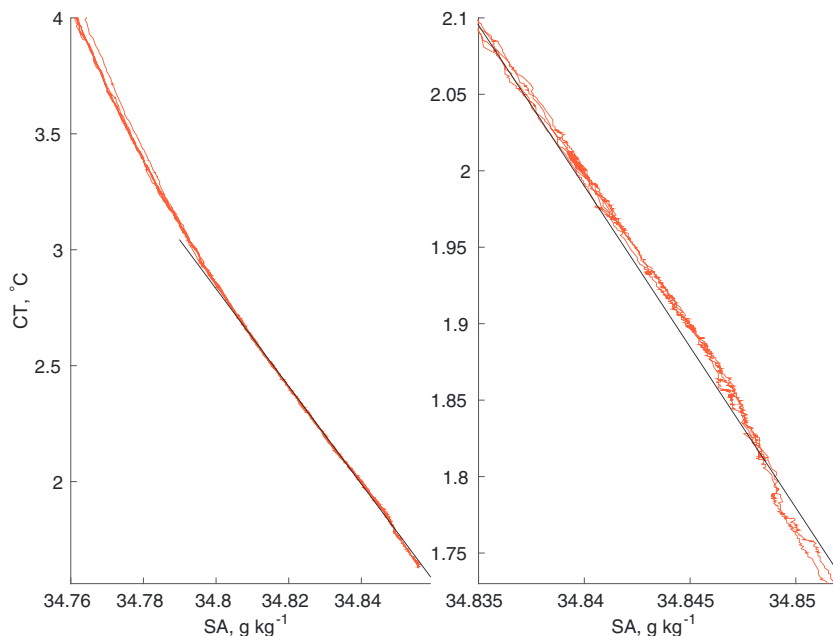


**Figure 10.** Temperature-salinity diagram at the Ecuador Trench with a linear fit for the data below 1,700 m ( $CT = 2.64 \text{ }^\circ\text{C}$ ).

the basin below 2200-m depth, other than through the southern boundary, the TS anomalies caused by the geothermal heating in the Panama Basin extend at least 500 m above the upper boundary of the abyssal water layer, which we estimated to be the neutral density surface of  $27.967 \text{ kg/m}^3$  located at the depths 2,680–3,000 m. As thickness of the abyssal water layer varies with topography from several hundreds to over thousands of meters, the TS anomaly caused by the geothermal heating extends much higher than 500 m when viewed from the bottom.

## 5. Summary and Conclusions

The Panama Basin is a perfect location to investigate the effect of geothermal heating on abyssal water transformation, as geothermal heating in the basin is about 3 times the global average. Laird (1971) was the first to argue that the increase of bottom temperature within the basin must be the result of geothermal heating, although this study did not observe the accompanying bottom salinity changes. Previous attempts to constrain the deep heat balance of the basin found large geothermal heatfluxes in comparison to the heat outflow through the Carnegie Ridge Saddle (Detrick et al., 1974). However, ours as well as historical studies (Lonsdale, 1977; Tsuchiya & Talley, 1998) indicate that deep water exchange through the saddle is very weak. Instead, most of the abyssal water that becomes lighter by accumulating geothermal heating in the basin flows out through the Ecuador Trench.

We have recalculated the heat budget for the Panama Basin. An estimated  $0.29 \pm 0.07 \text{ Sv}$  of abyssal waters pass into the basin through the Ecuador Trench and have a neutral density range,  $\Delta\gamma$ , between  $28.016 \text{ kg/m}^3$  and  $27.967 \text{ kg/m}^3$ . The total area enveloped by the upper boundary of abyssal water layer ( $\gamma_u = 27.967$ ) is estimated to be  $S = (3.8 \pm 0.2) \times 10^5 \text{ km}^2$  and gains the total geothermal heatflux of  $Q = (84 \pm 4) \times 10^9 \text{ W}$  with the average geothermal heatflux rate of  $220 \text{ mW/m}^2$ . With thermal expansion coefficient of  $\alpha = (1.5 \pm 0.15) \times 10^{-4} / \text{K}$  and a heat capacity of seawater of  $C_p = 3,992 \text{ J}\cdot\text{kg}^{-1}\cdot\text{K}^{-1}$ , geothermal heatflux contributes about  $0.13 \text{ Sv}$  to the total abyssal water transformation, using a formula  $\alpha/C_p \times Q/\Delta\gamma$ , which is about 50% of the total estimated inflow.

However, geothermal heating effect is very unequally distributed among different water masses. This study shows that about 65% of the total inflow is already transformed in the first 200 km downstream of the Ecuador Trench due to intense mixing accompanying the critical flow. Hence, the basin is filled with abyssal waters of a much narrower density range,  $[27.988 \text{ } 27.967] \text{ kg/m}^3$ , than inflow waters directly at the Ecuador Trench. Furthermore, the densest bottom waters have much smaller access to the bottom, compared to the lighter abyssal waters which have much larger bottom intercept areas (incrops) (Banyte et al., 2018). Large incrops result in a much larger total geothermal heating effect. As a result, while turbulent mixing downstream of the narrow passage can transform more than half of the densest abyssal waters into lighter waters, on the western side of the basin, where the lightest abyssal waters reside, geothermal heating contributes most of the abyssal water transformation.

Finally, the intense geothermal heating in the Panama Basin introduces new water masses with anomalous positive temperatures and salinities, revealed by the concave TS diagrams. All deep Panama Basin waters below 2,200 m have a characteristic geothermal heating-induced TS concave signature. Above 2,200 m the basin becomes much better ventilated by exchange pathways both through the southern as well as the eastern boarder. In conclusion, the thermodynamic effect of geothermal heating in the Panama Basin extends high up in the water column: at least 500 m above the abyssal water layer which is several hundred meters thick in most of the basin.

## References

- Adcroft, A., Scott, J. R., & Marotzke, J. (2001). Impact of geothermal heating on the global ocean circulation. *Geophysical Research Letters*, *28*, 1735–1738.
- Alford, M. H., Girton, J. B., Voet, G., Carter, G. S., Mickett, J. B., & Klymak, J. M. (2013). Turbulent mixing and hydraulic control of abyssal water in the Samoan passage. *Geophysical Research Letters*, *40*, 4668–4674. <https://doi.org/10.1002/grl.50684>
- Baker, E. T., & Massoth, G. J. (1987). Characteristics of hydrothermal plumes from two vent fields on the Juan de Fuca ridge, northeast Pacific Ocean. *Earth and Planetary Science Letters*, *85*, 59–73.
- Banyte, D., Morales Maqueda, M. A., Hobbs, R., Smeed, D. A., Megann, A., & Recalde, S. (2018). Geothermal heating in the Panama Basin. Part II: Abyssal water transformation. *Journal of Geophysical Research*. <https://doi.org/10.1029/2018JC013869>
- Bindoff, N. L., & McDougall, T. J. (1994). Diagnosing climate change and ocean ventilation using hydrographic data. *Journal of Physical Oceanography*, *24*, 1137–1152.
- de Lavergne, C., Madec, G., le Sommer, J., Nurser, A. J. G., & Garabato, A. C. N. (2016). On the consumption of Antarctic bottom water in the abyssal ocean. *Journal of Physical Oceanography*, *46*, 635–661.

### Acknowledgments

This research was supported in part by NSF grants OCE 1353114 and 1558797 to RPL and OCE. The NERC OSCAR project grant NE/I022868/1 (Morales Maqueda and Smeed, 2014) underpinned this work. The authors would like to thank the officers, crew, technicians, and scientists on board the RRS *James Cook* and RV *Sonne* during cruise JC112 and SO238. We are grateful to the Alvaro Morales Ramirez (Centro de Investigación en Ciencias del Mar y Limnología, Universidad de Costa Rica), Nancy Villegas Bolaños (Departamento de Geociencias, Universidad Nacional de Colombia), and Galo Quezada (Reserva Marina de Galápagos) for their invaluable help during the OSCAR project fieldwork. We also thank the “Ministerio de Ambiente y Energía”, Costa Rica, the Armada de la República de Colombia, and the Instituto Oceanográfico de la Armada de Ecuador (INOCAR) for the support provided to the said fieldwork. We are also grateful to Christine Peirce (Durham University) for processing the multibeam echo sounder data from SO238. The data from this campaign are made available through the British Oceanographic Data Centre ([bodc.ac.uk](http://bodc.ac.uk)).

- Detrick, R. S., Williams, D. L., Mudie, J. D., & Sclater, J. G. (1974). The Galapagos Spreading Centre: Bottom-water temperatures and the significance of geothermal heating. *Geophysical Journal of the Royal Astronomical Society*, *38*, 627–637.
- Downes, S. M., Hogg, A. M., Griffies, S. M., & Samuels, B. L. (2016). The transient response of Southern Ocean circulation to geothermal heating in a global climate model. *Journal of Climate*, *29*, 5689–5708.
- Emile-Geay, J., & Madec, G. (2009). Geothermal heating, diapycnal mixing and the abyssal circulation. *Ocean Science*, *5*, 203–217.
- Hofmann, M., & Morales Maqueda, M. A. (2009). Geothermal heat flux and its influence on the oceanic abyssal circulation and radiocarbon distribution. *Geophysical Research Letters*, *36*, L03603. <https://doi.org/10.1029/2008GL036078>
- Jackett, D. R., & McDougall, T. J. (1997). A neutral density variable for the world's oceans. *Journal of Physical Oceanography*, *27*, 237–263.
- Laird, N. P. (1971). Panama Basin deep water-properties and circulation. *Journal of Marine Research*, *29*, 226–234.
- Lonsdale, P. (1977). Inflow of bottom-water to the Panama Basin. *Deep Sea Research*, *24*, 1065–1101.
- Lonsdale, P. F., & Malfait, B. T. (1974). Abyssal dunes of foraminiferal sand on the Carnegie Ridge. *Geological Society of America Bulletin*, *85*, 1697–1712.
- McDougall, T. J., & Barker, P. M. (2011). *Getting started with TEOS-10 and the Gibbs Seawater (GSW) oceanographic toolbox*, pp. 28. Hobart, Tas: Marine and Atmospheric Research. SCOR/IAPSO WG127, ISBN 978-0-646-55621-5.
- Müller, R. D., Roest, W. R., Royer, J. Y., Gahagan, L. M., & Sclater, J. G. (1997). Digital isochrons of the world's ocean floor. *Journal of Geophysical Research*, *102*, 3211–3214.
- Murton, B. J., Baker, E. T., Sands, C. M., & German, C. R. (2006). Detection of an unusually large hydrothermal event plume above the slow-spreading Carlsberg Ridge: NW Indian Ocean. *Geophysical Research Letters*, *33*, L10608. <https://doi.org/10.1029/2006GL026048>
- Speer, K. G., & Rona, P. A. (1989). A model of an Atlantic and Pacific hydrothermal plume. *Journal of Geophysical Research*, *94*(C5), 6213–6220. <https://doi.org/10.1029/JC094iC05p06213>
- St Laurent, L. C., & Thurnherr, A. M. (2007). Intense mixing of lower thermocline water on the crest of the mid-Atlantic Ridge. *Nature*, *448*, 680–683.
- Stein, C. A., & Stein, S. (1992). A model for the global variation in oceanic depth and heat flow with lithospheric age. *Nature*, *359*, 123–129.
- Tsuchiya, M., & Talley, L. D. (1998). A Pacific hydrographic section at 88°W: Water-property distribution. *Journal of Geophysical Research*, *12*, 899–918.
- Whitehead, J. A., Leetmaa, A., & Knox, R. A. (1974). Rotating hydraulics of strait and sill flows. *Geophysical and Astrophysical Fluid Dynamics*, *6*, 101–125.